C. R. Mecanique 345 (2017) 712–723

Contents lists available at ScienceDirect

Comptes Rendus Mecanique

www.sciencedirect.com

A hybrid multi-objective imperialist competitive algorithm and Monte Carlo method for robust safety design of a rail vehicle

Mohamed Nejlaoui [a,*], Ajmi Houidi [b], Zouhaier Affi [a], Lotfi Romdhane [c]

[a] National School of Engineers, University of Monastir, Tunisia
[b] Higher Institute of Applied Sciences and Technology, Sousse, Tunisia
[c] College of Engineering, The American University of Sharjah, Sharjah, United Arab Emirates

ARTICLE INFO

Article history:
Received 9 December 2016
Accepted 28 May 2017
Available online 20 June 2017

Keywords:
Optimization
Rail vehicle
Curved tracks
Safety
Robust design
Uncertainty

ABSTRACT

This paper deals with the robust safety design optimization of a rail vehicle system moving in short radius curved tracks. A combined multi-objective imperialist competitive algorithm and Monte Carlo method is developed and used for the robust multi-objective optimization of the rail vehicle system. This robust optimization of rail vehicle safety considers simultaneously the derailment angle and its standard deviation where the design parameters uncertainties are considered. The obtained results showed that the robust design reduces significantly the sensitivity of the rail vehicle safety to the design parameters uncertainties compared to the determinist one and to the literature results.

1. Introduction

It is a common practice in a rail vehicle (RV) safety design to consider the nominal values only as input variables for design optimization. Nejlaoui et al. [1] took care of the RV security in quasi-static cases by using the Genetic Algorithm (GA) method. He and McPhee [2] treated a mono-objective optimization design of the RV derailment by using Genetic Algorithms. The objective function is a weighted combination of the angle of attack and of the ratio of the lateral force to the vertical force applied by each wheel on the rail. To evaluate the RV safety system, Eom and Lee [3] developed a sensitivity analysis of the parameters related to the derailment coefficients of track conditions. Banerjee et al. [4] used a model with 18 degrees of freedom to analyze the RV safety through determining the critical speed.

However, the RV design parameters (DPs) have usually an uncertainty around their nominal values due to the presence of variations in manufacturing, geometry, and material properties. To estimate the effect of DP uncertainty on the performance of a mechanical system, several methods have been described. In particular, the Monte Carlo Simulation (MCS) is a popular tool because of its relative precision and simplicity [5]. Araujo et al. [6] use the MCS method to estimate the uncertainty of surface emissivity, obtained by dual spectral infrared radiometry at ambient temperature. Motevalli et al. [7] applied a MCS approach to study the water inflow uncertainty impact on the performance of both single and multi-reservoir systems.

* Corresponding author. Fax: +216 73 500 514.
E-mail address: nejlaouimohamed@gmail.com (M. Nejlaoui).

http://dx.doi.org/10.1016/j.crme.2017.05.014
1631-0721/

Nomenclature

i	Index of wheelset	y_{ki}	Transversal displacement of the wheelset i of bogie k
j	Index of wheel.		
k	Index of bogie	y_k	Transversal displacement of the bogie k
g	The gravity constant	$\bar{y}$	Transversal displacement of the car body
G_{ki}	Wheelset center of mass	α_{ki}	Yaw angle of the wheelset i of the bogie k
G_k	Bogie center of mass	α_k	Yaw angle of the bogie k
$\bar{G}$	Car body center of mass	$\bar{\alpha}$	Yaw angle of the car body
m	Half wheelset mass	θ_k	Roll angle of the bogie k
$\hat{m}$	Bearing box body mass	$\bar{\theta}$	Roll angle of the car body
M	Bogie mass	θ_{ki}	Roll angle of the wheelsets ki
$\bar{M}$	Car body mass	V	The speed of the vehicle
N	Normal load by a wheel	K_u	Spring stiffness of the primary suspension in the direction u $(u = x, y, z)$
H	Vertical distance between the primary and the secondary suspension	$\bar{K}_u$	Spring stiffness of the secondary suspension in the direction u
h_0	Vertical distance between the primary suspension and G_k	d	Transversal distance between the primary suspension and G_k
δ	The rail inclination		
γ_0	Inclination of the tangent plan of contact wheel–rail with the horizontal	$\bar{d}$	Transversal distance between the secondary suspension and the car body center of mass
e_0	Half spacing of the track	R	Curvature radius of the wheel profile
γ_e	Equivalent conicity	R'	Curvature radius of the rail profile
R_c	Radius of curve	S	the normal force on the flange

Other works have studied the robust product design where uncertainties of the DP are considered. Cheng and Li [8] have developed a hybrid differential evolution and sequential quadratic programming method that ensures robust mechanical structures under uncertain DP. Kalantari et al. [9] have developed a hybrid robust evolutionary algorithm by combining the NSGAII process with a local search method. This strategy is used to optimize composite structures under an uncertain fiber angle and a lamina thickness. Bouazizi et al. [10] studied the robust optimization of a vibration absorber using the GA. The robustness, defined by the ratio of the mean value to the standard deviation, is treated as an objective function.

This paper deals with the multi-objective robust design optimization of a rail vehicle moving in short-radius curved tracks based on the safety criteria. A combined algorithm based on the Multi-objective Imperialist Competitive Algorithm (MOICA) and the MCS is proposed. The obtained results are compared to literature ones. In section 2, the dynamic model of the RV is reviewed and the safety criterion is defined. Section 3 deals with the determinist multi-objective design optimization of RV safety. Then, the authors show that the determinist optimal solutions can be seriously altered by DP uncertainties. In Section 4, a novel algorithm is developed and used in multi-objective robust optimization. The results are discussed and compared with literature results. Finally, some concluding remarks are presented in section 5.

2. Model of the RV system

The RV system is made of a rigid car body C, bogies C_k and wheelsets S_{ki}. The connection between these components is represented by the secondary and the primary suspensions. Each suspension is formed by a system of linear springs and dampers, which work in three directions (Fig. 1) [1,11].

The longitudinal symmetry of the RV system leads to the decoupling of lateral, vertical and longitudinal motions [1,11]. In this paper, we focus on the lateral dynamic behavior of the RV system. To simplify the analysis without reducing the accuracy of the model, we will consider only a quarter model of the RV (Fig. 1) [1,11]. Hence, the RV system has only eight degrees of freedom represented by the generalized coordinate vector $\mathbf{q}$:

$$\boldsymbol{q} = [\bar{y}, \bar{\alpha}, y_1, \alpha_1, y_{11}, \alpha_{11}, y_{12}, \alpha_{12}]^{\mathrm{T}} \tag{1}$$

In this study, the rail is assumed to be smooth and rigid. Moreover, due to the fact that the rail curve radius and the RV speed are constant, damping forces were found not to be important, compared to the elastic ones [1,11].

We may find the dynamic model of the RV system by applying the Lagrange method:

$$\frac{\mathrm{d}}{\mathrm{d}t}\left(\frac{\partial L}{\partial \dot{q}_i}\right) - \frac{\partial L}{\partial q_i} = Q_i \tag{2}$$

L is the Lagrangian function and Q_i represents the generalized forces applied to the system.

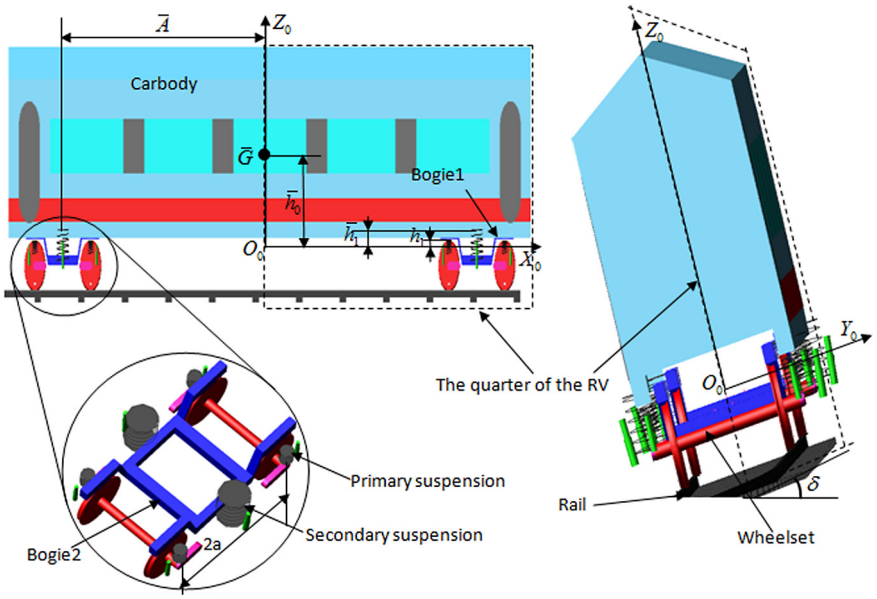

Fig. 1. The rail vehicle model.

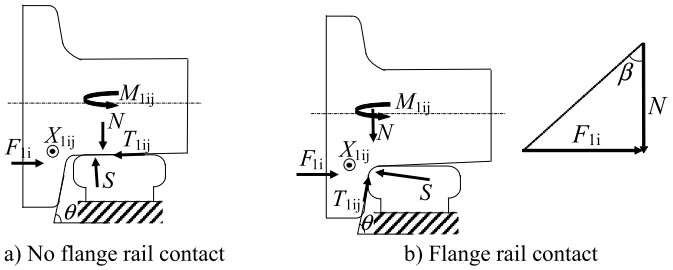

a) No flange rail contact b) Flange rail contact

Fig. 2. The wheel–rail contact forces.

The use of Eq. (2) gives us the following RV dynamic model:

$$\mathbf{A}(\mathbf{q})\mathbf{q} = \mathbf{b} \tag{3}$$

For more details, see [1,11]. The matrix **A** and the vector **b** are given in the appendix.

2.1. Safety modeling

The creep forces at the wheel–rail interface in longitudinal (X_{1ij}), in lateral (T_{1ij}) directions and a torque (M_{1ij}) (Fig. 2) are modeled based on Kalker's non-linear theory [1,2]. The derailment risk of the RV system can occur if the lateral force F_{1i} surpasses a certain limit. These forces F_{1i}, which are responsible for the derailment, can be identified through the algebraic equations of the analytical dynamic model [1,11]:

$$\begin{aligned} F_{1i} = {} & \sum_{i=1}^{i=2} K_y\left(y_1 - y_{11} - (-1)^i a\alpha_1 - y_{12}\right) - (-1)^i \bar{K}_x \frac{\bar{d}^2}{2a}\left(\tilde{\alpha}^* + \frac{y_1}{\bar{A}} - \frac{y_{11}-y_{12}}{2a} - \alpha_1 + \frac{\bar{A}}{R_c}\right) \\ & + \sum_{i=1}^{i=2}(-1)^i \frac{K_x d^2}{2a}\left(\alpha_1 - \alpha_{1i} + \frac{y_{11}-y_{12}}{2a} - (-1)^i \frac{a}{R_c}\right) + 2\chi C_{22}\alpha_{1i}\sum_i + (m+\hat{m})\gamma_{nc} + W\zeta y_{1i} \end{aligned} \tag{4}$$

C_{22} is Kalker's coefficient [2,11] and $\sum_i$, χ, W, ζ and γ_{nc} are defined in the appendix.

The analysis of the equilibrium forces in vertical and lateral directions gives:

$$\frac{F_{1i}}{N} = \frac{\tan\theta - \frac{T_{1ij}}{S}}{1 + \frac{T_{1ij}\tan\theta}{S}} \tag{5}$$

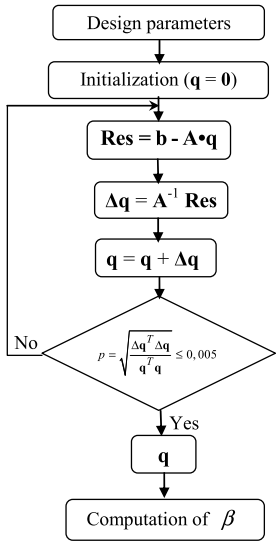

Fig. 3. The solving algorithm.

Table 1
Design variables and their search domains ([1,2] and [11]).

DP	K_u (N/m)	$\tilde{K}_u$ (N/m)	γ_e	$\tilde{M}$ (kg)	M (kg)
D(DP)	[10^6, 10^8]	[10^4, 10^6]	[0.02, 0.25]	[30000, 45000]	[3000, 3500]

According to the Coulomb law of friction, to be away from creep, the maximum of (T_{1ij}/S) cannot exceed the coefficient of friction μ. Therefore, at a given maximum contact angle $\theta_{\max}$, to avoid the derailment, we should have:

$$\frac{F}{N} \leq \frac{\tan\theta_{\max} - \mu}{1 + \mu\tan\theta_{\max}} \left(F = \max(F_{1i})\right) \tag{6}$$

This gives

$$\tan\beta \leq \frac{\tan\theta_{\max} - \mu}{1 + \mu\tan\theta_{\max}} \left(\tan\beta = \frac{F}{N}\right) \tag{7}$$

The minimization of the derailment angle β will be considered as the objective function.

2.2. The solving algorithm

The obtained model, defined in Eq. (3), is highly nonlinear. In order to solve the model in **q**, we developed an iterative algorithm based on Broyden's method [11,12] (Fig. 3). The value of β is calculated using Eq. (7).

3. Determinist optimization of the RV safety

At constant speed, the vehicle can circulate with different radii of curvature that increase the non-compensated lateral acceleration $\gamma_{nc} = \frac{V^2}{R_c} - g\delta$. Consequently, this increases the centrifugal forces. These forces can cause the derailment of the RV system, especially in short-radius curved tracks.

The goal of this work is to find the RV design vector parameters that minimize the objective function β. The minimization of the derailment angle β ensures the maximization of the RV safety for different motion scenarios characterized by R_c ($R_c \in$ [200 m to 500 m]).

In what follows, we will optimize the DPs that have the most significant effect on the dynamic behavior of the RV system. The search domains D(DP) of each DP are listed in Table 1. The other design variables of the RV are considered constant. Their values are given in [1,2,11].

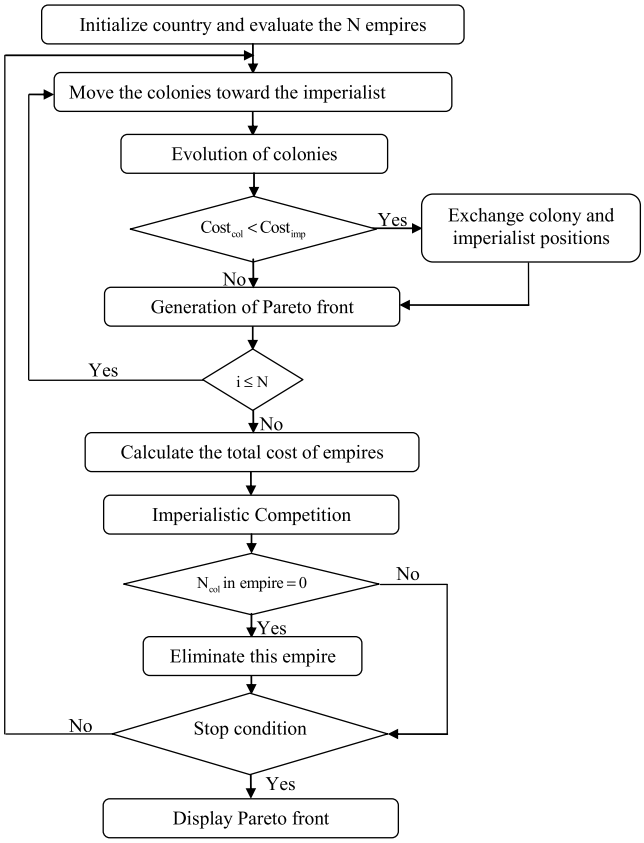

Fig. 4. The MOICA flowchart.

Thus, the optimization problem can be presented as follows:

$$\begin{cases} \text{Minimize} \quad \beta \\ \text{under the constraints:} \\ \quad \text{DP} \in \text{D(DP)} \\ \quad R_c \in [200, 250, 300, 350, 400, 450, 500] \\ \quad \beta \leq \beta_{\max} \end{cases}$$

For $\theta_{\max} = 75$ degrees [1] and $\mu = 0,31$ [2], in order to avoid the derailment $\beta_{\max} = 58$ degrees (Eq. (7)).

3.1. The optimization method

The multi-objective imperialist competitive algorithm (MOICA) is an evolutionary optimization method developed recently by [13]. The MOICA flowchart is shown in Fig. 4.

The MOICA begins with a generation of an initial population randomly. Each element of the population is a country. The power of a country, which is the counterpart of the fitness value in GA, is inversely proportional to its cost given by Eq. (8).

$$Cost_k = \sum_{j=1}^{r} \frac{|f_{j,k} - f_j^{\text{best}}|}{|f_j^{\max} - f_j^{\min}|} \tag{8}$$

r is the number of objective functions and $f_{j,k}$ is the value of the objective function j for the kth country. $f_j^{\max}$ and $f_j^{\min}$ are the maximum and minimum values of the objective function j in each iteration, respectively. f_j^{best} is the minimum or the maximum of the objective function according to the optimization process.

The powerful countries in the population are selected to be the imperialists, and the rest form the colonies of these imperialists. The normalized cost of the nth imperialist is given by [13,14]:

$$C_n = \max_i\{Cost_i\} - Cost_n \tag{9}$$

where $Cost_i$ and $Cost_n$ are the costs of the ith and the nth imperialist, respectively.

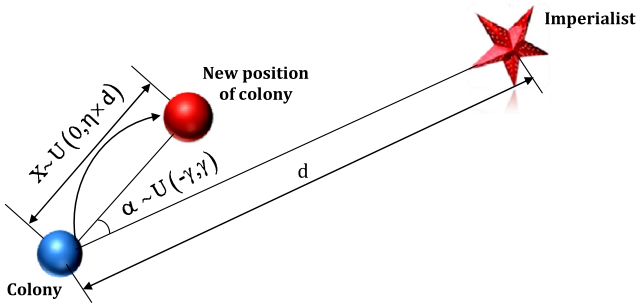

Fig. 5. Colonies moving toward their relevant imperialist.

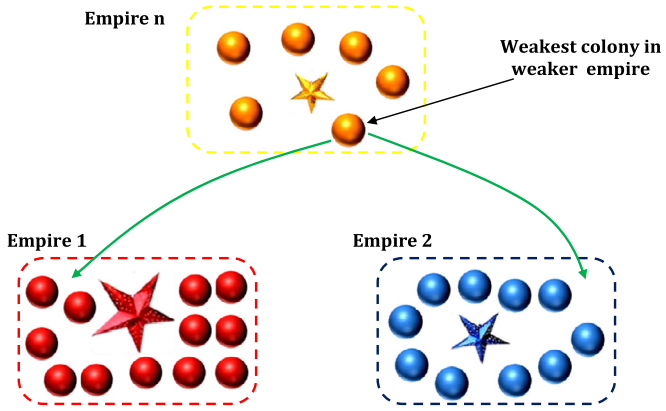

Fig. 6. Imperialistic competition.

The normalized power of the nth imperialist is calculated as:

$$P_n = \left| \frac{C_n}{\sum_i C_i} \right| \tag{10}$$

Due to the imperialists' powers, the colonies of the initial population are divided among them to form the initial empires. Each initial empire is composed of one imperialist and several colonies. After forming the initial empires, the colonies start moving towards their relevant powerful imperialist (Fig. 5). In this movement, α and X are numbers generated uniformly as $X \sim U(0, \eta \times d)$ and $\alpha \sim U(-\gamma, \gamma)$. d is the distance between the imperialist and the colony and η must be greater than 1. γ is a parameter representing the direction deviation [13,14].

In each empire, the multi-points crossover and the random replacement mutation operators enhance the colonies with a new one that can have more power. The evaluation of colonies and imperialists is based on the cost given by Eq. (8). The costs of the new colonies are compared with the cost of the imperialist. If any colony becomes more powerful than its imperialist, the imperialist and the colony are swapped. Then the fast non-dominated sorting approach [13,15] is used to rank the non-dominated imperialists in an archive to form the Pareto front.

The sum of an imperialist power and the average power of all its colonies gives the empire power. During the imperialists competition, all empires, based on their power, try to acquire the other empires colonies (Fig. 6). The weakest empires lose their colonies and collapse. The MOICA algorithm stops when all the weak empires collapse and only one powerful empire remains.

3.2. Results and discussion

The application of the optimization program, for different values of R_c, gives the results displayed in Fig. 7. One can notice that when the radius of curvature R_c increases, the derailment angle β decreases. In fact, the increase in R_c decreases the derailment force (from Eq. (4)) applied to the vehicle.

In what follows, we will analyze the evolution of the derailment angle as a function of the radius of curvature for three different optimized design vectors (1, 4 and 7), presented in Fig. 7. For each design vector, corresponding to solutions S1, S4 and S7 (Table 2), we show in Fig. 8 the curve (CSi) representing the evolution of β as a function of R_c.

One can note in Fig. 5 that the derailment phenomenon is more likely to occur when using the S4 and S7 design vector, even at 200 m. The RV system will be safe if it is constructed with the S1 design vector. Thus, the S1 optimal solution

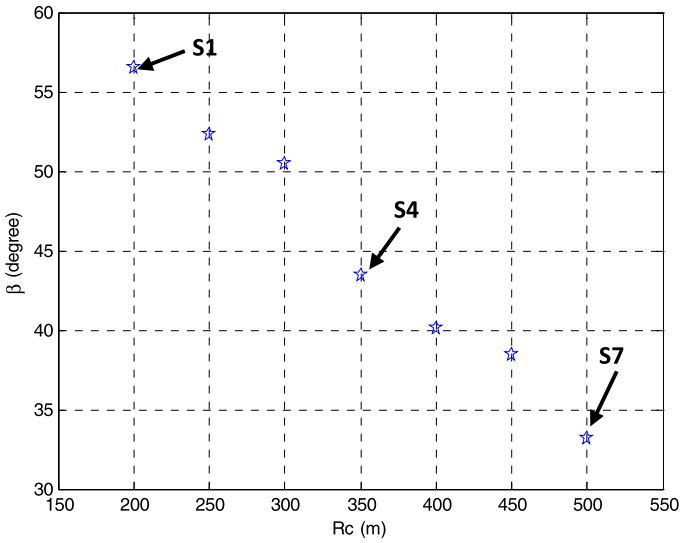

Fig. 7. Optimization results.

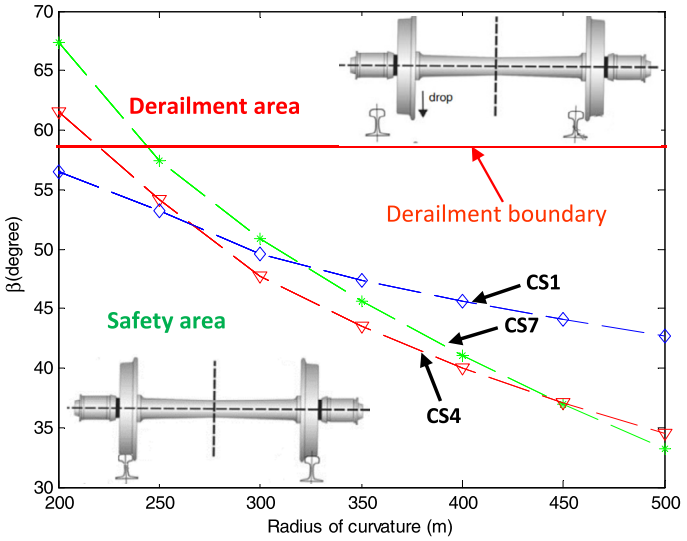

Fig. 8. Evolution of β as a function of R_c (for S1, S4 and S7 solutions).

Table 2
The design parameters corresponding to the chosen solutions.

	K_x (N/m)	K_y (N/m)	K_z (N/m)	$\bar{K}_x$ (N/m)	$\bar{K}_y$ (N/m)	$\bar{K}_z$ (N/m)	γ_e	$\bar{M}$ (kg)	M (kg)
S1	$1{,}33 \cdot 10^6$	$1{,}68 \cdot 10^6$	$1{,}88 \cdot 10^6$	$1{,}21 \cdot 10^4$	$1{,}73 \cdot 10^4$	$1{,}93 \cdot 10^4$	0,19	43520	3454
S4	$3{,}84 \cdot 10^6$	$4{,}13 \cdot 10^6$	$4{,}76 \cdot 10^6$	$4{,}29 \cdot 10^4$	$4{,}42 \cdot 10^4$	$6{,}01 \cdot 10^4$	0.13	41340	3219
S7	$6{,}78 \cdot 10^6$	$7{,}54 \cdot 10^6$	$8{,}82 \cdot 10^6$	$8{,}65 \cdot 10^4$	$7{,}98 \cdot 10^4$	$9{,}23 \cdot 10^4$	0,11	36747	3033

corresponds to a safe design vector of the RV system in the range of 200 to 500 m. However, for a more realistic analysis, the design parameters can present uncertainties around their nominal values. These uncertainties can generate variability of the RV safety evaluated by β. Therefore, the safety performances represented through the S1 optimal solution can often be altered by the design parameters uncertainties.

In what follows, we will study the effect of the design parameters uncertainties on the variability of the derailment angle β.

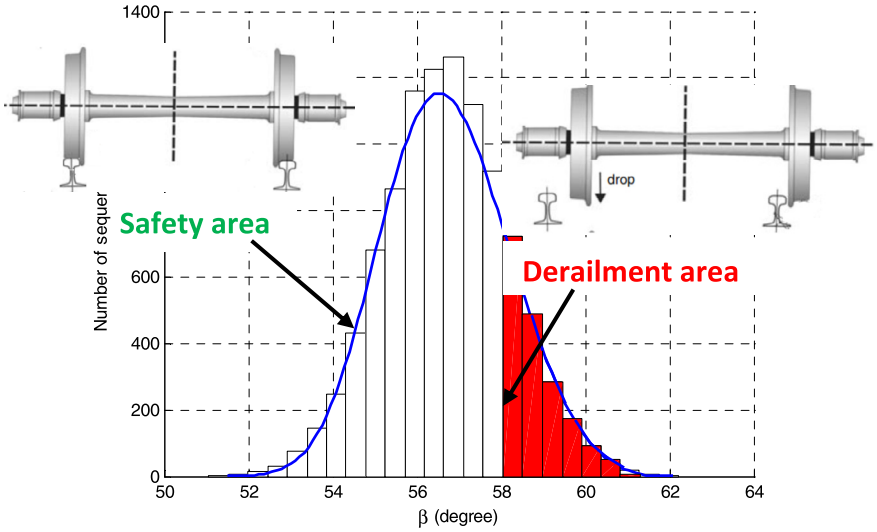

Fig. 9. Fluctuation of β to the DP uncertainties (S1 solution for $R_c = 200$ m).

3.3. The RV safety variability as a function of the design parameters uncertainty

In what follows, the variability of the optimized RV safety generated by the DP uncertainties will be estimated. Thus, the case of an optimal solution S1, given in Table 2, will be studied.

Each uncertain DP is presented by a normal distribution and characterized by a mean value and a standard deviation. The MCS is performed for every DP where each evaluation consists of a specified number of runs. For each MCS, all the determinist design variables are fixed at their nominal values and their uncertainty are selected randomly from their statistical distributions supposed to vary within $\pm 10\%$ of the specified nominal values [2].

With the MCS, we perform $n = 10^4$ simulations to determine the mean values $\bar{\beta}$ and the standard deviation σ. The evolution of the derailment angle β is presented in Fig. 9.

One can note that the derailment angle can reach up to 60° and the imposed constraint $\beta \leq \beta_{\max}$ is not satisfied. Consequently, by considering the DP uncertainties, the safety given by the determinist optimal solution S1 is no longer guaranteed. Therefore, one can conclude that the obtained determinist optimal solutions are not robust to the DP uncertainties.

A multi-objective robust design, where the sensitivity of the RV safety would be one of the objective functions, is needed.

4. Robust design of the RV safety

The robust design of the RV system should have the maximum of safety levels (defined by the minimum of $\bar{\beta}$) and also the minimum of safety variability generated by the DP uncertainty. This robustness can be quantified by the standard deviation σ of the objective function, i.e. high robustness of the solution means low standard deviation, for a given uncertainty of the DP. Consequently, the robust optimal design strategy can be expressed as follows:

$$\begin{cases} \text{Minimize} & \bar{\beta} \\ \text{Minimize} & \sigma \\ \text{Subject to:} & \bar{\beta} + 3\sigma \leq \beta_{\max} \\ & R_c \in [200, 250, 300, 350, 400, 450, 500] \\ & \text{DP} \in D(\text{DP}) \end{cases}$$

The constraint $\bar{\beta} + 3\sigma \leq \beta_{\max}$ imposes that the solutions are considered only if we have 99% confidence that the derailment angle does not exceed the maximum allowed derailment angle.

4.1. The MOICA–MCS algorithm

In this work, the MOICA–MCS Algorithm (Fig. 10) that combines the MOICA and the MCS is developed and used to solve this optimization problem to obtain robust solutions.

After the evolution stage, the MOICA sends a generation of countries to the MCS. The MCS performs n simulations for every country and sends back to the MOICA the mean values, $\bar{\beta}$, and its standard deviations, σ. Then these countries undergo the remaining steps of the MOICA algorithm.

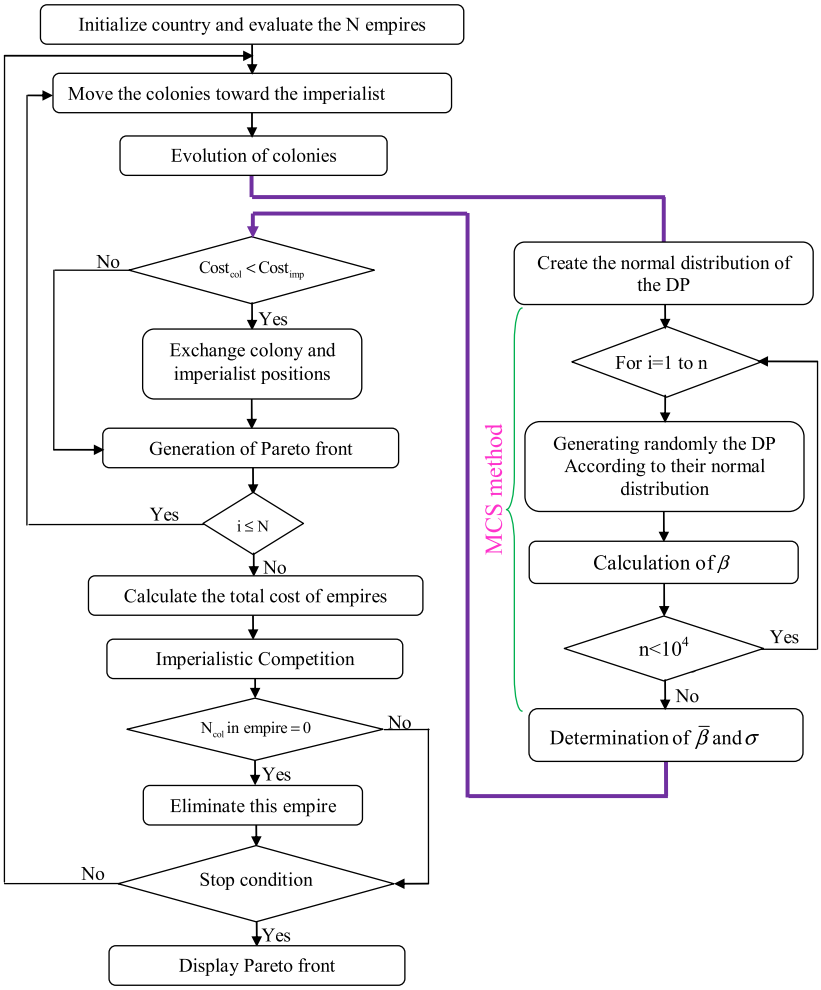

Fig. 10. The MOICA–MCS algorithm.

5. Results and discussion

Using the MOICA–MCS algorithm, we obtain the robust optimal solutions presented in Fig. 11. For each radius of curvature in the range of 200 to 500 m, we obtain a corresponding Pareto front. The Pareto front concept locates a set of non-dominated solutions. These solutions are called non-dominated because each one has, at least, one optimum (minimum/maximum) objective function [15–17]. To simplify the analysis, we present only the Pareto fronts corresponding to 200, 350 and 500 m in three dimensions and in top view (Fig. 11).

To better understand the particularity of the robust solutions, the design vectors of the three safest solutions (corresponding to low derailment angle values at each R_c) are given in Table 3.

For comparison reasons, we present in Fig. 12 the robust Pareto fronts with determinist results and with a set of bibliographic results.

The standard deviation of determinist and bibliographic solutions are determined by introducing their DP under the SMC. The values of $\bar{\beta}$ and σ are summarized in Table 4.

To compare the safety vulnerability of robust, determinist and literature solutions, we present in Fig. 13 their statistical distributions.

It is clear from Fig. 13 and Table 4 that the robust solutions present the lower fluctuations of the derailment angle compared to determinist results and to a result from the literature. In term of $\bar{\beta}$, one can note that the robust solutions keep about the same lower values given by the determinist results. Moreover, the robust solutions have the minimum values of σ compared to determinist and literature results. Based on this discussion, we can note that the robust design of the RV system has the maximum of safety levels (defined by the minimum of $\bar{\beta}$), and also the minimum of safety variability generated by the DP uncertainty.

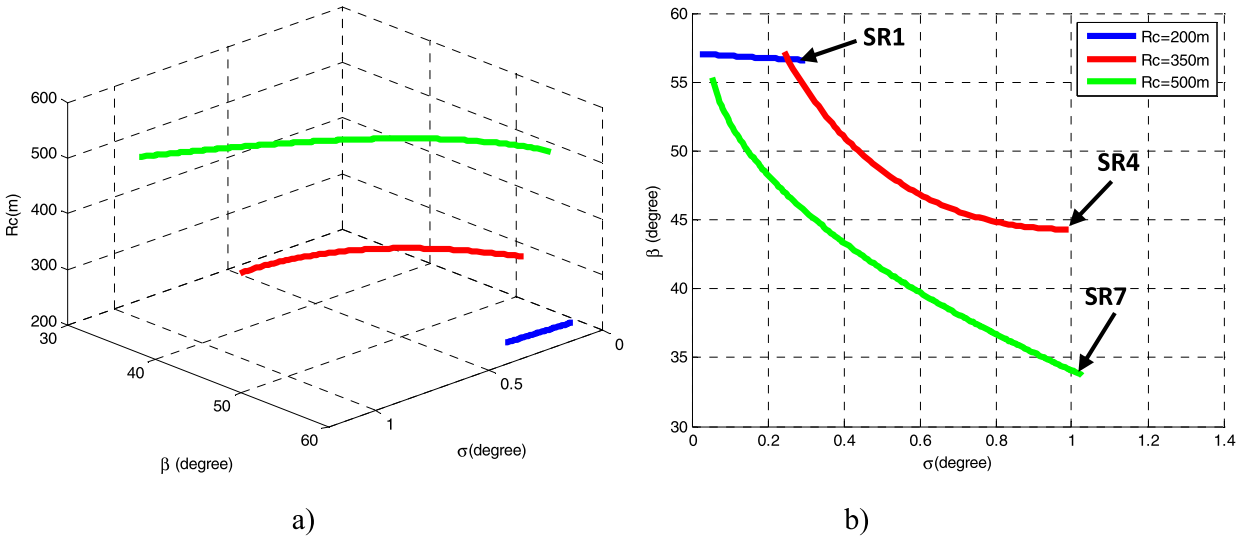

Fig. 11. Robust design; a) 3D view, b) top view.

Table 3
The design vectors of robust solutions SR1, SR4 and SR7.

	K_x (N/m)	K_y (N/m)	K_z (N/m)	$\tilde{K}_x$ (N/m)	$\tilde{K}_y$ (N/m)	$\tilde{K}_z$ (N/m)	γ_e	$\bar{M}$ (kg)	M (kg)
SR1	$1{,}02 \cdot 10^6$	$1{,}12 \cdot 10^6$	$1{,}23 \cdot 10^6$	$1{,}01 \cdot 10^4$	$1{,}18 \cdot 10^4$	$1{,}03 \cdot 10^4$	0,19	44520	3454
SR4	$1{,}12 \cdot 10^6$	$1{,}38 \cdot 10^6$	$1{,}08 \cdot 10^6$	$1{,}6 \cdot 10^4$	$1{,}23 \cdot 10^4$	$1{,}28 \cdot 10^4$	0 · 13	41012	3305
SR7	$1{,}24 \cdot 10^6$	$1{,}42 \cdot 10^6$	$1{,}9 \cdot 10^6$	$1{,}79 \cdot 10^4$	$1{,}32 \cdot 10^4$	$1{,}47 \cdot 10^4$	0,11	35547	3028

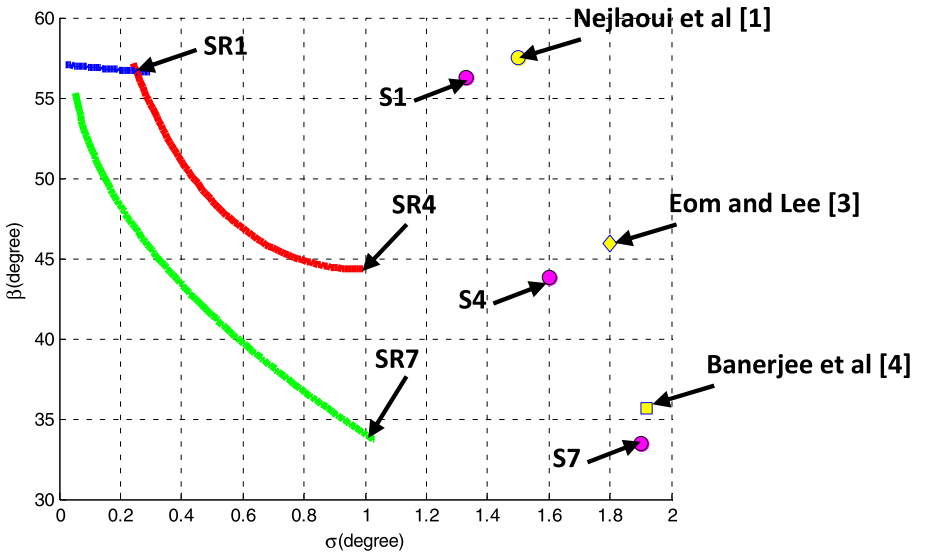

Fig. 12. Robust, determinist and bibliographic results.

Therefore, one can conclude that finding a determinist optimal solution is not sufficient. Additionally, one has to be sure that the obtained solution is robust enough to the uncertainty of the DP. When one thinks that it is true, one can think of this design as much better than those unchecked for the robustness to the uncertainty of their DP.

Figs. 11, 12 and 13 can be a valuable tool for the designer, since they can be used to choose the level of confidence of the chosen solution. If the designer has low confidence in his DP, he can favor the robustness of the solution by choosing low values for the standard deviation.

To have an idea of the computational time of the proposed algorithm, the objective functions and the different constraints are implemented under the Matlab software, according to the MOICA algorithm, and compiled using a computer with Cori7, 740 Qm, 1.74 GHz, RAM 8 GB. The execution time for the RV optimization (for $R_c = 350$ m) was about 93 and 58 s for the

Table 4
Values of $\bar{\beta}$ and σ for robust, determinist and bibliographic design.

	SR1	SR4	SR7	S1	S4	S7	Nejlaoui et al. [1]	Eom and Lee [3]	Banerjee et al. [4]
$\bar{\beta}$ (degree)	56.45	43.38	33.6	56.38	43.35	33.5	57.13	45.87	35.79
σ (degree)	0.29	0.96	1.02	1.33	1.6	1.9	1.42	1.8	1.92

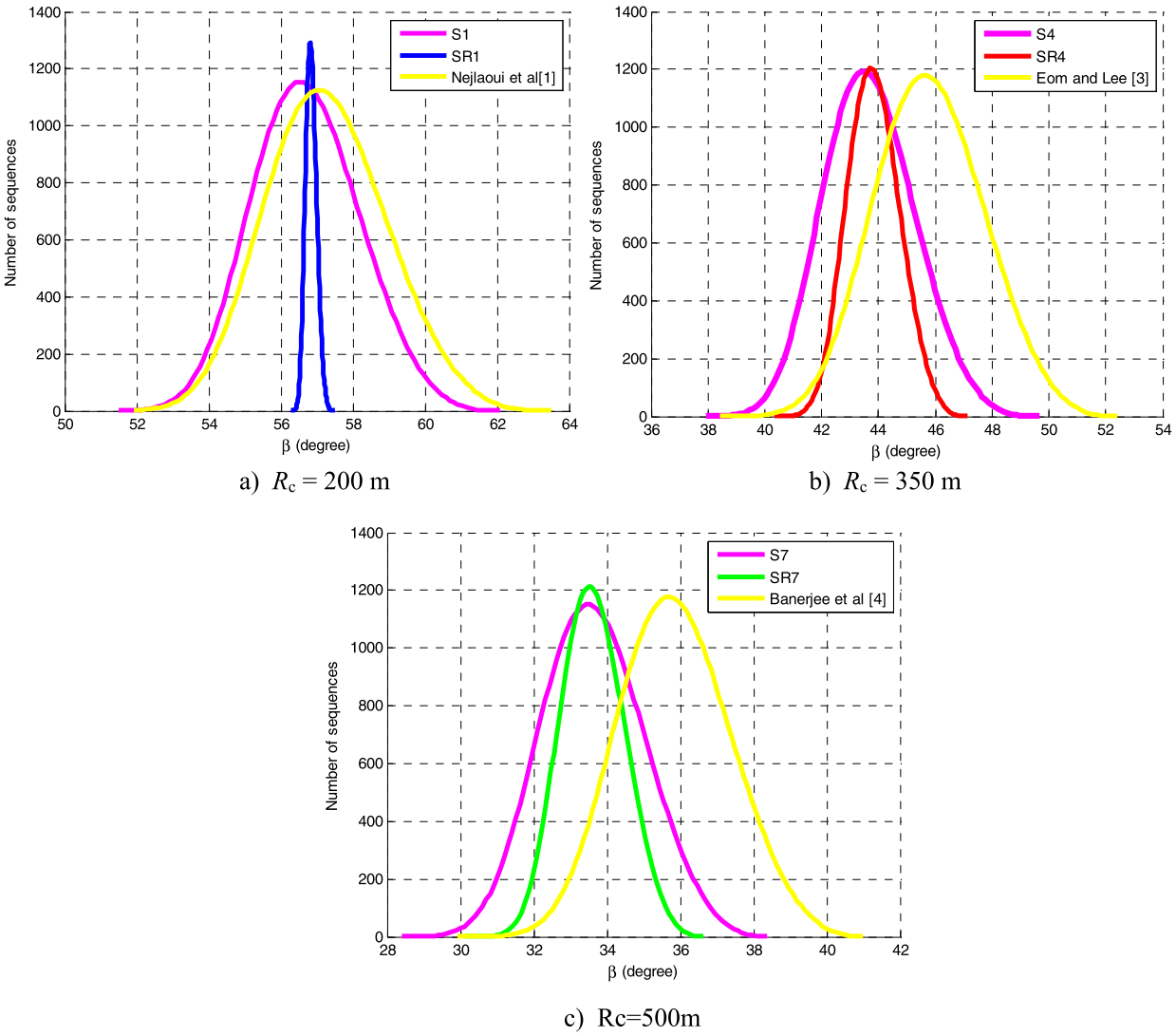

Fig. 13. Safety fluctuations of robust, determinist and bibliographic solutions.

robust and determinist cases, respectively. The execution time difference between the robust and the determinist cases is due to the time needed for the Monte Carlo simulation. In fact, 104 simulations are performed for each uncertain design vector, in order to quantify the effect of the design parameters uncertainties.

6. Conclusion

This paper introduced a multi-objective robust design optimization of the rail vehicle safety under uncertain design parameters. First, a determinist optimization design was conducted; where it was shown that the optimal determinist solution safety is highly sensitive to the design parameters uncertainties. An algorithm, which combines the multi-objective imperialist competitive algorithm and the Monte Carlo method, was introduced for the multi-objective robust design optimization of the rail vehicle safety where the standard deviation of the objective function is considered as a second objective function.

The obtained results showed that the robust design reduces significantly the sensitivity of the rail vehicle safety to the DP uncertainties compared to the determinist one and to the literature results.

The presented analysis could help the designer in his choice of the most adequate design parameters of a set of rail vehicle systems yielding the maximum robust safety.

Appendix

$$\mathbf{A}=\begin{bmatrix}
\bar{K}_y & \bar{K}_y\bar{A} & -\bar{K}_y & 0 & 0 & 0 & 0 & 0\\
\bar{K}_y\bar{A} & \bar{K}_x\bar{d}^2+\bar{K}_y\bar{A}^2 & \frac{\bar{K}_x\bar{d}^2}{A}-\bar{K}_y\bar{A} & -\bar{K}_x\bar{d}^2 & -\frac{\bar{K}_x\bar{d}^2}{2a} & 0 & \frac{\bar{K}_x\bar{d}^2}{2a} & 0\\
\bar{K}_y\bar{h}_1 & \bar{K}_y\bar{A}\bar{h}_1 & -\bar{K}_y\bar{h}_1 & 0 & 0 & 0 & 0 & 0\\
-\bar{K}_y & \left(\frac{\bar{K}_x\bar{d}^2}{A}-\bar{K}_y\bar{A}\right) & \left(\frac{\bar{K}_x\bar{d}^2}{A^2}+\bar{K}_y+2K_y\right) & -\frac{\bar{K}_x\bar{d}^2}{A} & \left(-\frac{\bar{K}_x\bar{d}^2}{2aA}-2K_y\right) & 0 & \left(\frac{\bar{K}_x\bar{d}^2}{2aA}-2K_y\right) & 0\\
0 & -\bar{K}_x\bar{d}^2 & -\frac{\bar{K}_x\bar{d}^2}{A} & \left(\begin{matrix}\bar{K}_x\bar{d}^2+2K_xd^2\\+2K_ya^2\end{matrix}\right) & \left(\bar{K}_x\frac{\bar{d}^2}{2a}+K_x\frac{d^2}{a}\right) & -K_xd^2 & \left(-\bar{K}_x\frac{\bar{d}^2}{2a}-K_x\frac{d^2}{a}\right) & -K_xd^2\\
-\bar{K}_y\bar{h}_1 & -\bar{K}_y\bar{A}\bar{h}_1 & \bar{K}_y\bar{h}_1 & 0 & -2K_yh_1 & 0 & -2K_yh_1 & 0\\
0 & -\frac{\bar{K}_x\bar{d}^2}{2a} & \left(-\frac{\bar{K}_x\bar{d}^2}{2a}-2K_y\right) & \left(\bar{K}_x\frac{\bar{d}^2}{2a}+K_x\frac{d^2}{a}\right) & \left(\begin{matrix}\bar{K}_x\frac{\bar{d}^2}{4a^2}+K_x\frac{d^2}{2a^2}\\+2K_y+W\zeta\end{matrix}\right) & \left(-K_x\frac{d^2}{2a}-2\chi C_{22}\Sigma_1\right) & \left(\begin{matrix}-\bar{K}_x\frac{\bar{d}^2}{4a^2}-K_x\frac{d^2}{2a^2}\\+2K_y\end{matrix}\right) & -K_x\frac{d^2}{2a}\\
0 & 0 & 0 & -K_xd^2 & -K_x\frac{d^2}{2a}+2e_0C_{11}\frac{\gamma_e}{r_0}\sigma_1 & \left(\begin{matrix}K_xd^2-W\gamma_0\varepsilon_0\\+2C_{23}\end{matrix}\right) & \frac{K_xd^2}{2a} & 0\\
0 & \frac{\bar{K}_x\bar{d}^2}{2a} & \left(\frac{\bar{K}_x\bar{d}^2}{2a}-2K_y\right) & \left(-\bar{K}_x\frac{\bar{d}^2}{2a}-K_x\frac{d^2}{a}\right) & \left(\begin{matrix}-\bar{K}_x\frac{\bar{d}^2}{4a^2}-K_x\frac{d^2}{2a^2}\\+2K_y\end{matrix}\right) & K_x\frac{d^2}{2a} & \left(\begin{matrix}\bar{K}_x\frac{\bar{d}^2}{4a^2}+K_x\frac{d^2}{2a^2}\\+2K_y+W\zeta\end{matrix}\right) & K_x\frac{d^2}{2a}-2\chi C_{22}\Sigma_2\\
0 & 0 & 0 & -K_xd^2 & \frac{-K_xd^2}{2a} & 0 & K_x\frac{d^2}{2a}+2e_0C_{11}\frac{\gamma_e}{r_0}\sigma_2 & \left(\begin{matrix}K_xd^2-W\gamma_0\varepsilon_0\\+2C_{23}\end{matrix}\right)
\end{bmatrix} \tag{A.11}$$

$$\mathbf{b}=\begin{bmatrix}\frac{\bar{M}}{4}\gamma_{nc} & 0 & \frac{M}{2}\gamma_{nc} & 2\bar{K}_x\bar{d}^2\frac{\bar{A}}{R_c} & (m+\hat{m})\gamma_{nc}-W\zeta y_0 & 2K_xd^2\frac{a}{R_c} & (m+\hat{m})\gamma_{nc}-W\zeta y_0 & -2K_xd^2\frac{a}{R_c}\end{bmatrix}^T \tag{A.12}$$

$$\gamma_{nc}=\frac{V^2}{R_c}-g\delta,\qquad \sigma_i=1-\frac{C_{11}}{3\mu N}\frac{\gamma_e}{r_0}y_{1i}^*+\frac{C_{11}^2}{27\mu^2N^2}\left(\frac{\gamma_e}{r_0}y_{1i}^*\right)^2 \tag{A.13}$$

$$\sum_i=1-\frac{C_{22}}{3\mu N}\alpha_{1i}+\frac{C_{22}^2}{27\mu^2N^2}\alpha_{1i}^2,\qquad \zeta=\frac{1}{(R-R')}\left(\frac{e_0+R\gamma_0}{e_0-r_0\gamma_0}\right)^2 \tag{A.14}$$

$$\varepsilon_0=(R+2r_0)\gamma_0-e_0,\qquad \chi=\frac{e_0}{(e_0-r_0\gamma_0)},\qquad W=\left(\frac{\bar{M}}{4}+\frac{M}{2}+m+\hat{m}\right)g. \tag{A.15}$$

References

[1] M. Nejlaoui, A. Houidi, Z. Affi, L. Romdhane, Multiobjective robust design optimization of rail vehicle moving in short radius curved tracks based on the safety and comfort criteria, Simul. Model. Pract. Th. 30 (2013) 21–34.
[2] Y. He, J. McPhee, Optimization of curving performance of rail vehicles, Veh. Syst. Dyn. 43 (2005) 895–923.
[3] B.-G. Eom, H. Sung Lee, Assessment of running safety of railway vehicles using multibody dynamics, Int. J. Precis. Eng. Man. 11 (2010) 315–320.
[4] N. Banerjee, A.K. Saha, R. Karmakar, R. Bhattacharyya, Bond graph modeling of a railway truck on curved track, Simul. Model. Pract. Th. 17 (2009) 22–34.
[5] C.I. Ossai, B. Boswell, I.J. Davies, Application of Markov modelling and Monte Carlo simulation technique in failure probability estimation—a consideration of corrosion defects of internally corroded pipelines, Eng. Fail. Anal. 68 (2016) 159–171.
[6] A. Araujo, S. Silvano, N. Martins, Monte Carlo uncertainty simulation of surface emissivity at ambient temperature obtained by dual spectral infrared radiometry, Infrared Phys. Technol. 67 (2014) 131–137.
[7] M. Motevalli, A. Zadbar, E. Elyasi, M. Jalaal, Using Monte-Carlo approach for analysis of quantitative and qualitative operation of reservoirs system with regard to the inflow uncertainty, J. Afr. Earth Sci. 105 (2015) 1–16.
[8] S. Cheng, M. Li, Robust optimization using hybrid differential evolution and sequential quadratic programming, Eng. Optim. 47 (1) (2015) 87–106.
[9] M. Kalantari, C. Dong, I.J. Davies, Multi-objective robust optimization of unidirectional carbon/glass fibre reinforced hybrid composites under flexural loading, Compos. Struct. 138 (2016) 264–275.
[10] M.L. Bouazizi, S. Ghanmi, R. Nasri, N. Bouhaddi, Robust optimization of the non-linear behavior of a vibrating system, Eur. J. Mech. A, Solids 28 (2009) 141–154.
[11] M. Nejlaoui, Z. Affi, A. Houidi, L. Romdhane, Analytical modeling of rail vehicle safety and comfort in short radius curved tracks, C. R. Mecanique 337 (2009) 303–311.
[12] J. Nocedal, S.J. Wright, Numerical Optimization, Springer-Verlag, ISBN 0-387-98793-2, 1999.
[13] B. Najlawi, M. Nejlaoui, Z. Affi, L. Romdhane, An improved imperialist competitive algorithm for multi-objective optimization, Eng. Optim. 48 (11) (2016) 1823–1844.
[14] E. Atashpaz-Gargari, C. Lucas, Imperialist competitive algorithm: an algorithm for optimization inspired by imperialistic competition, in: IEEE Congress on Evolutionary Computation, Singapore, 2007, pp. 4661–4667.
[15] R. Enayatifar, M. Yousefi, A.H. Abdullah, A.N. Darus, MOICA: a novel multi-objective approach based on imperialist competitive algorithm, Appl. Math. Comput. 219 (2013) 8829–8841.
[16] A. Sadollah, H. Eskandar, J.H. Kim, Water cycle algorithm for solving constrained multi-objective optimization problems, Appl. Soft Comput. 27 (2015) 279–298.
[17] S. Mirajelli, P. Jangir, S. Saremi, Multi-objective ant lion optimizer: a multi-objective optimization algorithm for solving engineering problems, Appl. Intell. 46 (2017) 79, http://dx.doi.org/10.1007/s10489-016-0825-8.